Regular Article

# Long-term physical evolution of an elastomeric ultrasound contrast microbubble

F. Domenici[a, *, 1], F. Brasili[a, 1], L. Oddo[a, 1], B. Cerroni[a], A. Bedini[c], F. Bordi[b], G. Paradossi[a]

[a] *Dipartimento di Scienze e Tecnologie Chimiche, Università degli Studi di Roma Tor Vergata, Via della Ricerca Scientifica 1, 00133 Roma, Italy*
[b] *Dipartimento di Fisica, Sapienza Università di Roma Sapienza, P.le A. Moro 5, 00185 Roma, Italy*
[c] *Dipartimento Innovazioni Tecnologiche e Sicurezza degli Impianti, Prodotti e Insediamenti Antropici (DIT), INAIL, Via di Fontana Candida 1, 00040 Monteporzio Catone, Italy*

ABSTRACT

*Hypothesis*

One of the main assets of crosslinked polymer-shelled microbubbles (MBs) as ultrasound-active theranostic agents is the robustness of the shells, combined with the chemical versatility in modifying the surface with ligands and/or drugs. Despite the long shelf-life, subtle modifications occur in the MB shells involving shifts in acoustic, mechanical and structural properties.

*Experiments*

We carried out a long-term morphological and acoustic evolution analysis on elastomeric polyvinyl-alcohol (PVA)-shelled MBs, a novel platform accomplishing good acoustic and surface performances in one agent. Confocal laser scanning microscopy, acoustic spectroscopy and AFM nanomechanics were integrated to understand the mechanism of PVA MBs ageing. The changes in the MB acoustic properties were framed in terms of shell thickness and viscoelasticity using a linearised oscillation theory, and compared to MB morphology and to nanomechanical analysis.

*Findings*

We enlightened a novel, intriguing ageing time evolution of the PVA MBs with double behaviour with respect to a crossover time of ∼50 days. Before, significant changes occur in MB stiffness and shell thickness, mainly due to a massive release of entangled PVA chains. Then, the MB resonance frequency increases together with shell thickening and softening. Our benchmark study is of general interest for emerging viscoelastomeric bubbles towards personalised medicine.

© 2018.

## 1. Introduction

Since their discovery, ultrasound contrast agents (UCAs) have expanded remarkably. Some of them are presently employed as invaluable and minimally invasive intravenous imaging tools which support early diagnosis [1–3]. Many developments have addressed the optimisation of their acoustic behaviour, targeting properties, cargo and release capacity as drug delivery systems, and their ability to support other imaging methods [1,4–7]. The complexity of tasks that have requested to turn UCAs into next-generation theranostic tools [1] represents the challenge to be tackled with an integrated approach, which requires expertise in medical imaging, biology, physics, and chemistry. From the physico-chemical standpoint, an UCA is a colloidal system that consists of a few micrometer-sized bubble encapsulating air or other functional gasses, suspended in an aqueous medium, and suitable for resonating at the megasonic fields. In this scenario, the platforms available to date are the following: protein-, lipid-, and polymer-shelled microbubbles (MBs) [1]. Since the albumin-shelled MB's development for purposes related to medical diagnostics [8],

several progresses have been made in the design of MBs, which are always aimed at increasing the stability and the mechanical properties offered by the MB shell. Lipid MBs are considered the most echogenic due to the elasticity of the monolayer shell that stabilises the hydrophobic gas in their core, although their shelf life is estimated to range from 6 h to 10 min (depending on the composition and the gas pressure of the physiological medium) due to processes involving gas leakage and colloidal instability [1,9]. The use of lipid MBs as drug carriers has also recently been proposed [1,9].

Usually, polymeric MBs show low US responsiveness, and in spite of a comparatively less flexible shell, they are considered more stable and suited to modifications of the shell, transforming a plain diagnostic tool into a theranostic system which is able to carry a drug and targeting molecules which comprise personalised medicine. Recently, biodegradable Poly (D,L-lactic acid)- and poly (D,L-lactic-co-glycolic acid)-shelled MBs have been developed, which show both high loading and release capacity of anthracyclines in tumoral cells [5,10]. Furthermore, it has been shown that such cavitating contrast agents can interact with cells in the vicinity of a plasma membrane, thus further increasing the release and the cell uptake of the drug [5]. A main issue concerning the polymer-shelled MBs is represented by the potential structural and chemical transformations [10], briefly summarised as an ageing process, that they undergo during their pro-

---

* Corresponding author.

*Email address:* fabio.domenici@uniroma2.it (F. Domenici)

[1] Equally contributing authors.

longed shelf life. The ageing of polymer MBs mainly involves some changes in the polymer network which surrounds and sustains the MB during storing time and cavitation. Undoubtedly, the understanding of ageing is pivotal for the optimisation of the acoustic properties, injectability, and biodistribution of UCAs [2,10,11]. To this end, valuable methodologies such as confocal [12] and near-field microscopies [13–15], together with acoustic spectroscopy [16,17], can be used and combined to detect morphological, structural, and, thus, functional fine alterations on the MB's wall at the liquid interface. Nevertheless, the literature has still been found to lack long-term studies in this respect.

In this work, the experimental and theoretical efforts have been focused on a novel polymeric UCA based on poly(vinyl alcohol) PVA shells that encapsulate air, which have been recently developed [18]. The PVA-shelled MBs are the product of a site-specific splitting reaction of the head-to-head sequences of the polymer backbone that gives rise to polymer sub-chains having reactive aldehydes, followed by an acetalisation reaction, thus enabling the crosslinking of the PVA chain. By running the reaction at the water/air interface that is obtained by foaming the solution of PVA, it is possible to separate a floating material made of air-encapsulated PVA shells. In previous works, it has been highlighted that despite exhibiting a thick shell of a few hundred nanometres, these MBs have an echogenicity comparable to SonoVue® UCAs [19], which is often taken as reference UCA in similar studies. The reason behind this is the chemical cross-linking of PVA, which transforms the polymer MB into an elastomer that is suitable for use in linear as well as nonlinear ultrasound (US) imaging methods. The resonant frequency falls to ∼10 MHz (against about 1–2 MHz of lipid ones), which is useful for diagnostics [20]. In combination with the much higher stability in the blood pool as compared with the respective lipid counterpart, PVA-shelled MBs have been gaining interest as valuable UCAs with great potential as multifunctional devices. In this respect, the strict interconnection between some pivotal multifunctional applications of our PVA MBs and their own peculiar crosslinked-PVA structure has been proven (e.g. the possibility of modifying the external surface of the shell, the targeting ability, and the biodistribution) [7,21]. From the compelling translational opportunities that the class of micro-structured PVA materials offers in biomedical engineering and theranostics, what emerged was the essential need to clarify how ageing affects the acoustic and structural properties of PVA-shelled MBs.

The main focal point of the work addressed herein lies in integrating the attenuation and the phase velocity of US that interacts with PVA MBs, together with optical and atomic force micro-spectroscopy, to probe and successfully figure out the geometrical, viscoelastic, and surface morphology of the shells over time. Our results have allowed to assess a time window for the optimal use and storage of PVA MBs as UCAs.

## 2. Materials and methods

### 2.1. Materials

Poly(vinyl alcohol) (PVA) with a number-average molecular weight, determined by membrane osmometry, of $30,000 \pm 5000$ g/mol, and a weight-average molecular weight of $70,000 \pm 10,000$ g/mol, determined by static light scattering were taken; sodium (meta)periodate ($NaIO_4$), fluorescein isothiocyanate isomer I (FITC), and dimethylsulfoxide (DMSO) were also taken as Sigma-Aldrich (Milan, IT) products. Water with Milli-Q purity grade ($18.2$ MΩ·cm) was produced using a PureLab Classic (ELGA LabWater, High Wycombe, UK) deionisation/purificaton apparatus.

### 2.2. Microbubble synthesis

In accordance with the previous literature [22], air-filled elastomeric PVA MBs were prepared by cross-linking telechelic PVA, whose chain terminals consist of aldehyde groups, in order to obtain cyclic acetals that would provide high stability to the shell [23–26]. Briefly, 4 g of PVA was added in 200 ml of Milli-Q water. The suspension was stirred at 80 °C until complete PVA dissolution was observed. 0.380 g of sodium (meta)periodate was added to the solution and the oxidation reaction was carried out at 80 °C for 1 h with constant stirring. After cooling the solution to room temperature, vigorous stirring for 2 h at 8000 rpm by an Ultra-Turrax T-25 (IKA, Staufen, D) equipped with a Teflon-coated tip generated a fine foam of cross-linked telechelic PVA, which acts both as colloidal stabiliser and air-encapsulating agent. This avoids the coalescence phenomena and the need of constant pressurisation (while using hydrophobic gases such as $SF_6$ or perfluorocarbons), both of which affect the width of the MB's size distribution. Floating MBs were separated from solid polymer debris (see also ESI, Fig. S1) by repeated washings in separatory funnels and stored without size filtering in Milli-Q water for further use. These washing steps were carried out till the 15th day from the start of the synthesis. Control measurements showed that in this period the acoustic response of the MBs was unstable (see also Section 2.4); the acoustic monitoring of the system as a function of the ageing time was therefore performed starting from the end of the washing steps. Thus, a homogeneous population of MBs was obtained (see also Section 4.1).

### 2.3. Fluorescent labelled microbubbles

FITC was used for the fluorescent tagging of the PVA MBs. In a typical labelling reaction, 40 µl of the dye (5 mg/ml in DMSO) was added to 1 ml MB suspension, whose number density varied between $1 \times 10^8$ ml$^{-1}$ and $5 \times 10^8$ ml$^{-1}$. MBs were gently shaken and, after being left for 1 h in the dark at room temperature, were washed by centrifugation (1000 rpm, 10 min). After the reaction, FITC was found to be covalently bound to the PVA shell by forming thiocarbamate groups. The floating MBs were resuspended in Milli-Q water. This purification step was repeated several times until excess FITC was removed.

### 2.4. Optical microscopy

The number density and the size distribution of PVA MBs were assessed at varying times by phase contrast and confocal microscopy, respectively (see Fig. S2 and Table S1). In order to determine the MB's number density, a Neubauer cell counting chamber (BRAND, Wertheim, D) was used and the counting method was adopted for MBs. An Eclipse Ti-E inverted optical microscope (Nikon, Florence, IT) with a Plan Fluor 20× objective (Nikon) was focused on the MBs inside the counting chamber. The number density was calculated by dividing the number of counted MBs by the volume of the chamber. MBs were counted with the aid of the freeware software Image J (http://imagej.nih.gov/ij/).

To determine the MBs' size distribution, PVA shells were tagged with FITC and confocal images of the equatorial plane were collected by a Confocal Laser Scanning Microscope (CLSM, Eclipse Ti-E, Nikon, Tokyo, Japan) using a Plan Apo 60× oil immersion objective (Nikon) and a Spectra Physics (Santa Clara, California, USA) Ar+ ion laser (488 nm) as the excitation source. The average outer diameter and the standard deviation were determined for each ageing day, analysed on a population of ∼200 MBs using the Nikon software EZ-C1 (version 3.9). The effect of ageing on the shell thickness $t$, which

is independent of the MB radius $R_o$ as previously reported [27], was also estimated by comparative analysis of the fluorescence intensity spatial profiles acquired on the newer (day 15) and the older (day 75) MB populations (see Fig. S3).

### 2.5. Acoustic response

Measurements of attenuation and phase velocity were carried out in triplicate using the setup shown in Fig. S4. In this configuration, a liquid sample of pure water, saline water, or contrast agent suspension was placed in a $2 \times 2 \times 4$ cm glass chamber at room temperature. The suspension was continuously and gently stirred by the action of a magnetic stirrer. The chamber had a liquid-tight opening on two opposite sides, so that an emitting and a receiving transducer could be placed in the liquid for the test. All measurements were taken using two flat wide-band V311 (Olympus, Milan, IT) transducers for emission and reception. The two transducers were separated by a distance $z = 2$ cm. To investigate the dispersion characteristics, ultrasonic signals were produced by means of a waveform generator with frequencies ranging from 0.5 to 20 MHz, in the form of consecutive sinusoidal bursts with 4 µs steps (250 kHz burst frequency). The received signals were digitised at 1 GS/s by random interleaved sampling and processed by comparison with the signals coming from a Milli-Q water reference medium. The normalised MBs attenuation coefficient $\alpha(\omega)$, defined according to Eq. (1), was determined as a function of frequency by subtracting the reference signal from that of the inspecting beam while propagating through the MBs' suspension:

$$\alpha = -\frac{1}{z} \ln\left(\frac{I}{I_0}\right),\tag{1}$$

where $I$ is the measured acoustic intensity and $I_0$ is the intensity at $z = 0$. Since the signal differed from the reference only because of the presence of MBs in the sound path, contributions from the glass chamber and the effects of the transducer's frequency response were compensated. All steps were controlled by the software platform LabView Transmission (National Instruments, Austin, Texas, USA). Both the emitting and the receiving transducer were calibrated by means of a needle hydrophone (Precision Acoustics, Dorchester, UK) with sensitivity between 371 mV/kPa and 496 mV/kPa in the range of the considered frequencies. For each frequency, the signal was driven by an input voltage of 6 $V_{pp}$. The output, measured in water at a distance of 2 cm from the transducer (the same as the distance between the transducers in the sample chamber), showed that the generated peak negative pressure (PNP) was never higher than 14 kPa. In terms of the orders of magnitude, this value was twice lower than the pressure fracture threshold of PVA MBs ($\sim$1.2 MPa) [28], and it was chosen to work under a very low and linear MB oscillation regime. It was indeed demonstrated [29] that such a linear regime was also maintained by working at higher pressures of one order of magnitude ($\sim$160 kPa). The maxima values of the spatial peak temporal average intensity ($I_{SPTA}$) and the mechanical index (MI) were 1.5 mW/cm$^2$ and 0.0047, respectively.

Before each measurement, the MB dispersion under investigation was kept again overnight in a separatory funnel which allowed the bubbles to float. In this way, any precipitated pellet was discarded to avoid interferences in the acoustic measurements and the floating MBs were resuspended in fresh Milli-Q water. After this washing step and prior to performing the experiments, $n_{MB}$ was determined using the counting method described in Section 2.3 (see Fig. S2). The sample chamber was therefore filled with 17 ml Milli-Q water and appropriate amounts of freshly washed MBs' stock suspension (generally $n_{MB} \sim 2 \times 10^8$ ml$^{-1}$) were pipetted into the chamber to obtain a

series of dilutions with increasing number density of the MBs, typically from $4 \times 10^4$ ml$^{-1}$ to $1 \times 10^6$ ml$^{-1}$.

Preliminary control measurements (not shown) pointed out that MBs exhibit highly variable attenuation response to the applied US field up to the 15th day from their synthesis. This means that for several days a prolonged washing protocol is needed to extract a population of MBs having reproducible properties. The washing steps described in Section 2.1 were therefore scheduled and the acoustic attenuation of PVA MBs was monitored afterwards over a time period of 60 days (from day 15th to day 75th) (see also Section 2 of ESI, Figs. S5 and S6). Each attenuation profile shows the average of seven consecutive measurements. The repeatability of measurements under US stimulation was successfully assessed by the small standard deviation of the average profile (see Section 4.2). It accounts for the high stability of the MBs under low US stress and their instrumental sensitivity.

The measured phase velocities were analysed at the frequency of 0.5 MHz. As stated in Section 3.2, under these conditions the acoustic response of the system is dominated by the elastic properties of the polymeric shell and the velocity scales linearly with the volume fraction $\phi$ of the dispersed MBs. The PVA bulk modulus, $K_{shell}$, can be therefore extracted by a linear fit of the phase velocity as a function of $\phi$ and converted into the shear modulus, $G_s$. According to Section 3.1, acoustic attenuation profiles were analysed using the Hoff model [30] to extrapolate the resonance frequency $\omega_0$ and the viscous damping coefficient $\delta$ of the MBs. Using the PVA shear modulus obtained from the phase velocity analysis and the MB size measured by CLSM, it was therefore possible to evaluate the shell thickness $t$ and the viscosity $\mu_s$.

The fitting of phase velocity and attenuation curves was performed using the Wolfram Mathematica V10.1 software. The goodness of the parameters of each fit was evaluated in terms of the reduced $\chi^2$ of the nonlinear solutions.

### 2.6. Atomic force microscopy

PVA MBs dispersed in water were deposited onto cleaned flat hydrophilic silicon substrates. If not stated otherwise in Section 4.3, the samples were washed before deposition to avoid the coating of the eventual PVA debris. Atomic Force Microscopy (AFM) analysis on plain PVA MBs was performed using a Dimension Icon microscope equipped with a Nanoscope V Controller (Bruker AXS, Fitchburg, Wisconsin, USA), CNIS, Sapienza University of Rome.

Images of different sizes with a resolution of $512 \times 512$ pixel were acquired in tapping mode at room temperature both in air and water environments, using a cantilever with a spring constant ($k_c$) of 40 N/m and 5 N/m, respectively. The MBs' size measured by AFM corresponds to the height with respect to the silicon surface.

Point-shoot force curve profiles were acquired in water with force thresholds ranging from $\sim$1 nN to $\sim$30 nN and a drive frequency of $\sim$200 kHz. Measurements were based on the proportionality between the cantilever deflection $\delta_c$ and the z-piezo displacement $Z$ [31,32]:

$$\delta_c = \frac{k_s}{k_c + k_s} Z,\tag{2}$$

where $k_s$ is the spring constant of the sample. Force-distance measurements on the hard silicon substrate ($k_s \gg k_c$, hence $\delta_c \approx Z$) allowed us to directly measure the lever deflection and calibrate its sensitivity to 64.6 nm/V. Afterwards, the spring constant of the sample was determined using Eq. (2), and $k_s$ could be expressed in terms of the tip-sample contact area, the Young modulus ($E$), and the Poisson ratio ($\nu$) of the sample [33]:

$$k_s = 2a \frac{E}{1 - \nu^2} Z, \tag{3}$$

where $a$ is the radius of the contact area. An exact estimate of $\nu$ should account for the polymer structure that is actually involved and, more importantly, for the elastomer share of the operating compression, which in turn depends on the polymer shape as well as on the entity of the stress involved. For an isotropic elastomer undergoing low solicitation, such as the shell of our MBs under the stress condition applied by the AFM measurement, the Poisson ratio can be reasonably assumed to be equal to that of a rubbery material with $\nu = 0.48$ [34].

A model is therefore required to express $a$ as a function of the applied force and, therefore, to extrapolate $E$ values from force curves. We employed the Derjaguin-Müller-Toporov (DMT) model [35], described in Section 3.3, to this end. Each value reported is the average of at least three independent measurements that are acquired on different MBs. The Young modulus of MBs, extrapolated by AFM, is related to the shear modulus $G_s$ of the PVA shell through the following equation [36]:

$$G_s = \frac{E}{2(1 + \nu)}. \tag{4}$$

Images and force curves were acquired by Nanoscope 8.1 in triplicate. 6 to 10 frames per measurement were analysed by NanoScope Analysis software (Bruker AXS).

## 3. Theoretical background

### 3.1. Acoustic attenuation model

A simple analytical model is used to interpret the MBs' attenuation curves in terms of the morphological and mechanical properties of the PVA shell and, thereby, to explain the evolution in terms of their echogenicity levels. In this regard, according to our experimental conditions (see Section 2.5), we assumed that the PVA shell behaves as a pure elastomer in a linear regime. In this framework, the MB shell undergoing US exhibits minor radial oscillations and a fundamental harmonic response only. Variations of the shell thickness $t$ in the linear regime are very small and, through both the constant shell volume constrain and the radial symmetry, they coherently follow those of the MBs' external radius $R_0$. In other words, we hypothesise that the dynamics of MB oscillation is well described by a single independent variable $R$. In this respect, to employ a mathematically convenient limiting model, we invoked the linearized Hoff acoustic theory [30] that accounts for the small oscillation dynamics of MBs with thin shells [37,38]. In order to account for the thick PVA shells of our MBs, we removed the thin shell approximation $t \ll R_0$, yielding $V_{shell}/V_{core} \approx 3t/R_0$), where $V_{shell}$ and $V_{core}$ are the volumes of the PVA shell and the gas core, respectively [30,37]. In this way, it was possible to derive a more rigorous analytical expression that could fit our experimental results. As reported in Section 4.2, the shell thickness values provided using this model fall between 200 nm and 400 nm, in striking similarity with existing literature [12,27,40,41]. Interestingly enough, the comparison with the linearized Hoff model shows that the viscoelastic values are not affected significantly by the thin shell approximation except for $t$ (see Fig. S7 of ESI). As a result, the overall values of $t$ became a little oversized when the thin shell model was employed.

According to such a linearized "thick shell model", the MB shell is characterised by a shear modulus $G_s$ and a viscosity $\mu_s$. The linear oscillations in a liquid with density $\rho_l$ and viscosity $\mu_l$ (for water, $\rho_l = 1$ g/cm$^3$ and $\mu_l \approx 0.89$ mPa·s) are described in terms of their resonance frequency $\omega_0$ and a viscous damping coefficient $\delta$:

$$\omega_0 = \sqrt{\frac{1}{\rho_l R_0^2} \left( 3\kappa p_0 + 4G_s \frac{V_{shell}}{V_{core}} \right)}, \tag{5}$$

and

$$\delta = \frac{4}{\omega_0 \rho_l R_0^2} \left( \mu_l + \mu_s \frac{V_{shell}}{V_{core}} \right), \tag{6}$$

where $\kappa$ is the polytropic exponent of air at room temperature ($\kappa = 1$, reasonably supposing an isothermal process) [30] and $p_0$ is its equilibrium pressure, considered equal to the pressure in the surrounding liquid ($p_0 = 1$ atm). According to the Hoff theory, the scattering and the thermal contributions to damping are neglected here [30]. The expression for the extinction cross section $\sigma$ of a single MB as a function of the normalised frequency $\Omega = \omega/\omega_0$ is given by the following equation:

$$\sigma(R_0, \Omega) = 4\pi R_0^2 \frac{c_0 \delta}{R_0 \omega_0} \frac{\Omega^2}{(1 - \Omega^2)^2 + \delta^2 \Omega^2}, \tag{7}$$

where $c_0$ is the speed of sound in the liquid, obtained by measurements in the absence of MBs. The attenuation $\alpha(\omega)$ of a MB suspension can be calculated by integrating the extinction cross section over the MB population. However, as reported in Section 4.1, in our experiments the size distribution of PVA MBs resulted as being very tight and did not change significantly over time, allowing to properly extrapolate cross section profiles from the measured acoustic attenuation assuming that a population of MB had the same radius $R_0$:

$$\sigma(R_0, \Omega) = \frac{\alpha(\Omega)}{n_{MB}}. \tag{8}$$

The overall assumptions considered here lead to an adherent fitting of the experimental data (see Fig. 2, panel A of Section 4.2) in the relevant frequency range, thus allowing a reliable comparative analysis in function of the MBs' ageing time.

### 3.2. Sound velocity in a bubbly liquid

The sound velocity $c$ in a liquid is altered by the presence of MBs, resulting, below the resonance frequency, in a significant lowering even at small volume fraction of MBs $\phi \ll 1$ [42]. In the inhomogeneous bubbly liquid, it can be expressed as follows:

$$c = \sqrt{\frac{K}{\rho}}, \tag{9}$$

where $K$ and $\rho$, the effective bulk modulus and the density respectively, are given in terms of the average of the two components (liquid, $l$, and bubbles, $MB$) of the medium:

$$\frac{1}{K} = (1 - \phi) \frac{1}{K_l} + \phi \frac{1}{K_{MB}}, \tag{10}$$

$$\rho = (1 - \phi) \rho_l + \phi \rho_{MB}. \tag{11}$$

In our case, the surrounding liquid is water thus $\rho_l = 1 \, \text{g/cm}^3$ and $K_l = \rho_l c_0^2$, where $c_0$ is the velocity of sound in water. The density $\rho_{MB}$ of MBs can be calculated by a volume-weighted average between the densities $\rho_{shell}$ of the PVA polymer shell ($1.2 \, \text{g/cm}^3$, accounting for water contribution) [22,43] and $\rho_{core}$ of the core gas. Assuming $\rho_{core} \ll \rho_{shell}$ yields, we get the following equation:

$$\rho_{MB} = \rho_{shell} \left[ 1 - \left( \frac{R_o - t}{R_0} \right)^3 \right]. \tag{12}$$

Noteworthy is the fact that at frequencies well below the resonance, the acoustic response of MBs is characterised by quite a low level of attenuation, even for high number densities, which can be ascribed to the scattering process [44]. It is therefore interesting to study the velocity of sound as a function of $\phi$ in this regime. According to the analyses reported in the literature on similar systems, the presence of an elastomeric shell characterised by high stiffness (shear modulus $G_s \sim \text{MPa}$) drives the interaction of MBs with the US field [45,46]. Therefore, in the presence of both crosslinked polymer-shelled MBs and low-frequency US, $K_{MB}$ can be replaced (<4% percentage error) in Eq. (10) by the bulk modulus of the shell, $K_{shell}$. A first-order expansion in $\phi$ of Eq. (9), combined with Eqs. (10) and (11), yields the following expression for the sound velocity in the bubbly liquid [30,47]:

$$c = \sqrt{\frac{K}{\rho}} \cong c_0 \left\{ 1 + \phi \left[ 1 - \frac{1}{2} \left( \frac{K_l}{K_{shell}} + \frac{\rho_{MB}}{\rho_l} \right) \right] \right\}, \tag{13}$$

The MBs volume fraction can be expressed in terms of their number density $n_{MB}$:

$$\phi = \frac{4}{3} \pi R_0^3 n_{MB}, \tag{14}$$

while the relation between the shear modulus and the bulk modulus of the shell is expressed by the following equation:

$$G_s = \frac{3}{2} \frac{1 - 2\nu}{1 + \nu} K_{shell} \tag{15}$$

### 3.3. Derjaguin-Müller-Toporov theory

AFM nanomechanical analysis of PVA MBs was performed according to the DMT model, suitable for experiments with low adhesion and small tip radii, which neglects plastic deformations and describes the tip and the sample as continuous elastic media [32,35]. Tip deformations are in accordance with the Hertz theory [48], where the geometry of a spherical tip of radius $R_0$, in contact with a rigid flat surface, is assumed. Additional adhesion forces acting between the two bodies which lie outside the contact region are taken into account, characterised by an adhesion work $w$. The radius of the contact area corresponding to an external load force $F$ is expressed as follows:

$$a = \sqrt[3]{\frac{3R_0}{4E^*} \left( F + 2\pi R_0 w \right)}, \tag{16}$$

where $E^*$ is the effective Young modulus given in terms of the Young moduli and the Poisson ratios of the two bodies, by the following [49]:

$$\frac{1}{E^*} = \frac{1 - \nu^2}{E} + \frac{1 - \nu_t^2}{E_t}, \tag{17}$$

where the subscript $t$ stands for the cantilever tip. The second term in Eq. (17) can be neglected if $E \ll E_t$, as in the case of the surface of a MB. Adhesion forces alone produce a finite area of contact $a_0$ even at zero load forces, as given by the following equation:

$$a_0 = \sqrt[3]{\frac{3\pi R_0^2 w}{2E^*}}. \tag{18}$$

If an external load is applied, $a$ increases, while for negative loads it diminishes until it reaches zero, in correspondence with the pull-off force:

$$F_{pullout} = -2\pi R_0 w. \tag{19}$$

## 4. Results and discussion

### 4.1. Size analysis

After their synthesis, PVA MBs in aqueous suspension underwent several washing steps, repeated for 15 days, in order to remove debris and the excess unbound FITC added during the fluorescent labelling of the shells. Colloidal stabilisation of such a system is primarily due to the amphiphilic nature of the PVA (hydrophilic –OH groups and hydrophobic –CH$_2$ groups) and the presence of polymer chains protruding into the bulk medium, which prevents particle coagulation [39]. These air-filled, cross-linked MBs display a shelf life of many months, showing very low gas permeability [12]. However, with time, a tiny amount of white precipitate can accumulate at the bottom of the vials containing the MBs' stock suspensions (Fig. S1). For this reason, in order to allow the proper comparison of measurements over time, immediately before each experiment the MBs were washed once again and their number density was measured (see Fig. S2).

As stated by Eq. (5), the resonance frequency of a MB depends on its radius $R_0$ and on the ratio between the volume of the shell and that of the core. The average external MB diameters and their distribution were therefore monitored over time for the entire period (60 days) over which the acoustic characterisation was carried out. The obtained values are reported in Table S1 of ESI. In Fig. 1, representative CLSM images and the corresponding size distributions are shown for the 15th and the 75th days. The average external diameters, calculated on populations of ~200 MBs, were found to be $4.3 \pm 0.7$ and $4.2 \pm 0.8 \, \mu\text{m}$, respectively. This means that the MBs population holds its narrow size distribution with no change in the average size value.

It is interesting to provide an experimental evaluation of the shell thickness of the MBs as a function of their ageing time. Nevertheless,
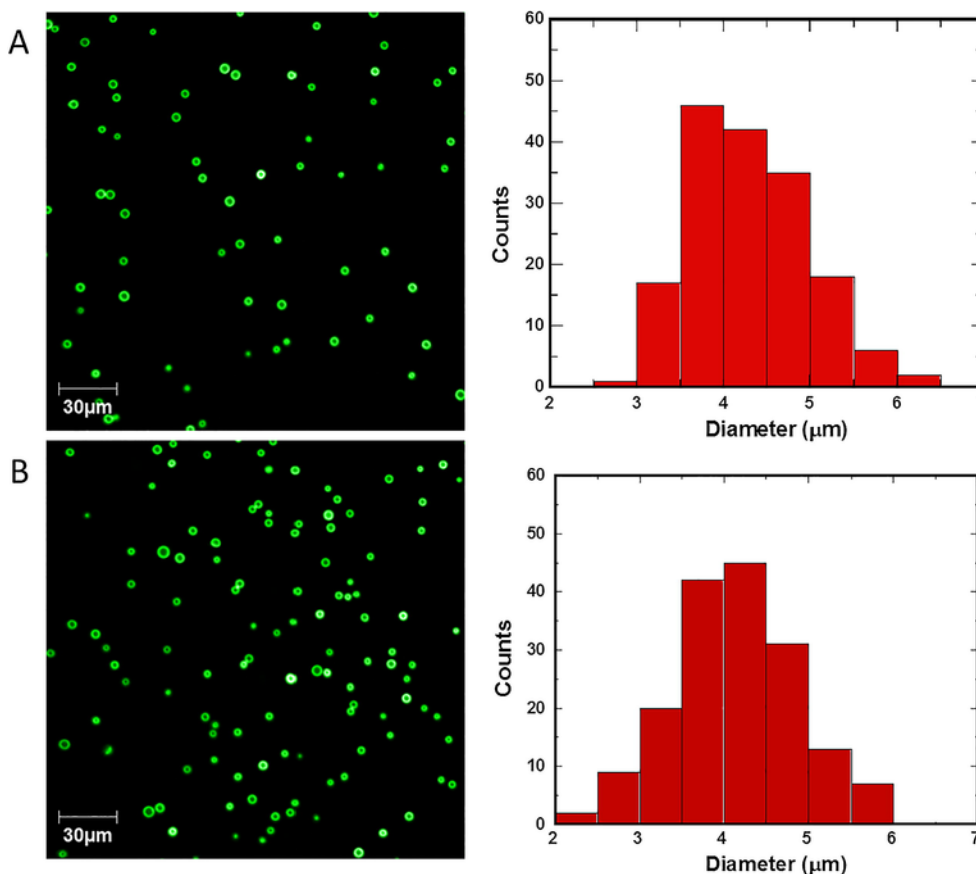
**Fig. 1.** Representative CLSM images on the left and corresponding size distributions on the right of the FITC-labelled PVA MBs, acquired in the 15th (A) and the 75th day (B) after their synthesis. The average external diameters were found to be $4.3 \pm 0.7\,\mu m$ and $4.2 \pm 0.8\,\mu m$, respectively.

the values obtained by CLSM lie at the limit of the optical resolution (of about 180 nm) and a complementary technique is, therefore, required to extrapolate an accurate trend [50]. A comparative analysis of the 15th and the 75th ageing days (see Fig. S3), corresponding to the maximum range being studied, showed a clear and reproducible lowering of the shell thickness by about 14%, from $640 \pm 15$ nm to $548 \pm 15$ nm, while the internal radius of MBs remained unchanged (<0.5% variations). We may infer that this variation involves a loss of material from the MBs' wall at the water interface. As a result, the shell thicknesses became systematically overestimated with respect to the values obtained through other techniques [12,27], probably due to a contribution to the fluorescence of PVA fibrils protruding outside the shell surface [7]. A more accurate evaluation of the long-term evolution of the shell thickness is reported in Section 4.2.

To understand whether the PVA MBs are destructured over time, their number densities were followed over time and are shown in Fig. S2. The MB count was performed according to Section 2.4. After 15 days, no significant decrease of MBs was observed over time until 55th day. Thereafter, a slight decrease may have occurred.

### 4.2. Acoustic attenuation and phase velocity

Despite cross-linked PVA MBs in aqueous suspension exhibiting a longer shelf life than lipid MBs, physico-chemical modifications of the polymer can occur, affecting the shell thickness and the viscoelastic properties with consequent alteration of the bubbles' acoustic response. Since bubbles suspended in an acoustic field absorb as well as scatter energy, the resulting attenuation of the incident US beam can be measured and analysed to obtain information not only on

MBs' acoustic behaviour but also about their viscoelastic properties. Achieving this information over time is a prerequisite for the employment of PVA MBs as US contrast agents.

In this framework, we measured the acoustic attenuation and the US phase velocity spectra in the 0.5–20 MHz frequency range at varying number densities of MBs dispersed in MilliQ water. Representative sets of spectra acquired at the 15th ageing day are reported in Fig. S5. We selected the number densities which showed a linear response of the attenuation peak maxima, as shown in Fig. S6. In this interval, the slope of the linear plot defines the value of the acoustic extinction cross section at the resonance $\sigma(\omega = \omega_0)$ of the PVA MBs at a fixed ageing time, which depends on the viscoelastic structure of the polymer shell according to Eq. (7). As shown in Fig. S6, $\sigma(\omega = \omega_0)$ varies with ageing time, pointing out significant modifications in the mechanical properties that are involved in the acoustic response of MBs.

Proceeding from this observation, in order to define the effects of the ageing time on the acoustic and mechanical properties of the system, it is necessary to analyse the evolution of the US attenuation and of the phase velocity spectra according to Sections 3.1 and 3.2, respectively. In Fig. 2, for each ageing time ranging between 15 and 75 days, the extinction cross section (panel A) and the phase velocity (panel B) experimental trends are reported, superimposed with the correspondent analyses. From the best fit according to Eqs. (7) and (13), the overall time set of MB parameters ($\omega_0$, $G_s$, $\mu_s$, and $t$) is carried out and reported in Table 1. The bulk modulus $K_{shell}$ of the PVA shell can be easily extracted from the study of the US phase velocity, which in the presence of MBs depends on the US frequency (Fig. S5, panel B). As mentioned in Section 3.2, it is interesting to analyse the
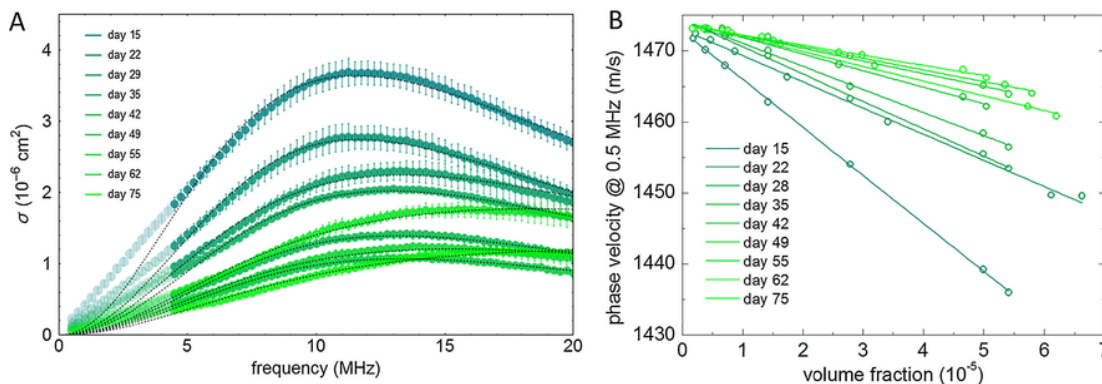
**Fig. 2.** Cross section (A) and phase velocity (B) profiles for the different ageing times that are analysed, from 15 to 75 days. The corresponding best fit curves, according to the models described in Section 3, are superimposed. Each profile contains the average of seven consecutive measurements. The corresponding small standard deviation values account for the high stability of the MBs under low US stress.

**Table 1**
Fitting parameters obtained by the acoustic response analysis as a function of ageing time.

| Ageing time (days) | $\omega_0$ (MHz) | $G_s$ (MPa) | $\mu_s$ (mPa·s) | $t$ (nm) |
|---|---|---|---|---|
| 15 | 11.57±0.04 | 0.10±0.01 | 31±2 | 390±20 |
| 22 | 11.67±0.03 | 0.17±0.01 | 44±3 | 350±20 |
| 29 | 12.83±0.05 | 0.17±0.01 | 41±3 | 350±20 |
| 35 | 12.85±0.05 | 0.19±0.01 | 45±4 | 340±20 |
| 42 | 13.12±0.05 | 0.26±0.01 | 59±5 | 240±10 |
| 49 | 13.24±0.05 | 0.35±0.02 | 77±6 | 210±10 |
| 55 | 14.03±0.07 | 0.38±0.01 | 74±4 | 260±10 |
| 62 | 15.7±0.1 | 0.42±0.03 | 73±7 | 310±30 |
| 75 | 18.9±0.4 | 0.44±0.02 | 63±6 | 350±20 |

sound velocity as a function of the MBs' volume fraction $\phi$ at frequencies well below the resonance, where the acoustic attenuation is very low. To this end, we extrapolated the phase velocities at 0.5 MHz, where a significant dependence on $\phi$ was observed and the acoustic response of the system was dominated by $K_{shell}$ [30]. In these conditions, the velocity scales linearly with $\phi$ according to Eq. (13). This allowed us to point out the values of $K_{shell}$ and, by means of Eq. (15), calculate the shear modulus $G_s$ of the shell as a function of the ageing time (Table 1).

Moreover, from the analysis of the evolution of the extinction cross section profiles, given by the average of the attenuation profiles normalised to the corresponding MB number density, it is possible to extrapolate the resonance frequency $\omega_0$ and the viscous damping $\delta$ of the PVA shell. Combining the $G_s$ values obtained from the analysis of the phase velocity with Eqs. (5) and (6) yields the shell thickness $t$ and the polymer viscosity $\mu_s$. The calculated values (Table 1) are in line with the Church model simulations and the experiments previously reported in the literature [40,41,45] and show an overall decrease in the shell thickness, which corroborates the hypothesis put forth by the CLSM investigation (Section 4.1).

The values of the MB parameters carried out from the fit are shown in Fig. 3 as a function of their ageing time. The time evolution appears characterised by two stages, separated by a crossover time of ~50 days. Before, the resonance frequency (panel A) remains approximately stable, whereas the increasing trend of $G_s$ (panel B) and $\mu_s$ (panel C) reflects the lowering of the shell thickness $t$ (panel D). Apparently, this indicates that the higher the ageing time of the MBs, the stiffer the PVA shell. To understand this, it is important to stress that, according to Section 2.5, before each measurement the samples are washed and separated from any PVA debris. Therefore, the increase in shell "rigidity" may be due to either the loss of a sub-population of MBs or a change in the MB shell assembly. As shown in Fig. S2, the

number density of MBs remains constant at least until the 55th day of ageing. Indeed, a high endurance over time is provided by the crosslinking of PVA chains made of cyclic acetals which are stable in water under environmental conditions (pH 6.5, at 25 °C) [23–26]. Nevertheless, the existing non-crosslinked PVA fraction (called entangled PVA chains) of the shell can be released from the surface of the MBs (and removed by washing). This would entail an increase of the weighting fraction of the crosslinked polymer and, hence, in the stiffness of the effective elastomer constituting the echogenic MB shell [51,52]. Notice that the overall thickness variation pointed out by the acoustic analysis strongly supports both the optical analysis shown in Fig. S3 and the AFM measurements reported in Section 4.3. Thus, the significant decrease in the thickness of the PVA shells seems consistent with a partial structural loss of mass, which might be due to the release of a shell fraction made up of non-crosslinked PVA chains.

As the ageing proceeded after the 50th day, we observed a second evolution stage. The rapid increase of the resonance frequency is associated with a slowing and the arrest of the increasing trend of $G_s$ and $\mu_s$, while an apparent increase of the average thickness occurs. In recent X-ray microspectroscopy and digital holographic microscopy studies [12,27,43] the presence of a sub-population of MBs partially filled with water has been highlighted. We hypothesise that after about 50 days after the synthesis, the release of non-crosslinked PVA chains becomes irrelevant and the observed time evolution is mainly due to variations in the MB population after each washing step. Specifically, the volume fraction of MBs partially filled with water becomes significant enough to cause a reduction of the average attenuation of the overall sample dispersion. In other words, according to the literature [12,27,43], we are confident that the existence of MBs with "defected" shells (i.e., porous or partially covered PVA shells) allow the water to access the MB nucleus and swell the polymer shells, thus behaving as an echogenic system with limited activity. The observed increase of the shell thickness (Fig. 3, Panel D) may be consistent with the presence of such "defected MBs". The presence of MBs exhibiting "defected" surface has found experimental support in the AFM analysis reported in Section 4.3.

It is also worth noting that from the 62nd day the variations in thickness and mechanical parameters shown in Fig. 3 are no longer significant (a plateau may have been reached) (Fig. 3, panels B, C, and D). We hypothesise that when the amount of water entering the shell of these unstable MBs is enough to induce them to precipitate from the water dispersion, they can be separated (removed). We assume that it is at this ageing time at which the unstable MBs tend to separate from the "population" of echogenic MBs, and can be removed by washing. In support of our hypothesis, a slight reduction of
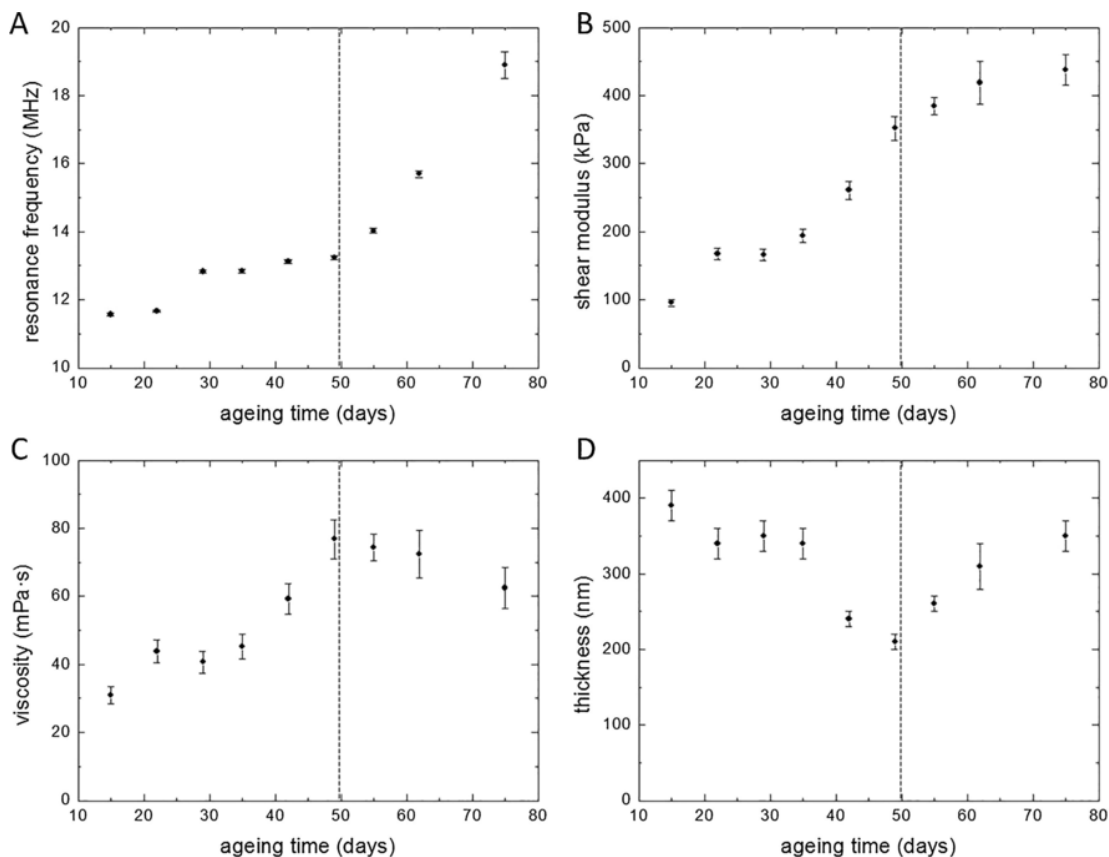
**Fig. 3.** The values of the resonance frequency $\omega_0$ (A), the shear modulus of the PVA shell $G_s$ (B), the shell viscosity $\mu_s$ (C), and the shell thickness $t$ (D), obtained from the analysis of the acoustic response as a function of ageing time. The dashed line represents the crossover time between the two evolution stages: at first (until 50th day) the ageing is dominated by the release of non-crosslinked PVA chains, and then by the removal of MBs with "defected" shells.

MBs' number density was actually observed from the 62th day onwards (Fig. S2).

### 4.3. AFM analysis

Topographic and nanomechanical characterisation of PVA-shelled MBs was performed by AFM according to Section 2.5, at the 15th and 75th ageing days. Representative images and force curves are shown in Fig. 4, panel A and B respectively, and the measured quantities are reported in Table 2. The shape and size of the MBs slightly differ from those shown in Fig. 1 that were gathered by CLSM analysis. According to the literature [7], the slight distortion observed in the MBs' shape, from spherical to elliptical, occurs due to the MBs' interaction with the substrate surface and with the cantilever tip. In fact, with respect to a perfectly spherical geometry observed in bulk, the AFM topograph shows a vertical reduction (the MB height decreases from ~4 to ~3 μm), together with a horizontal size increase.

Interesting enough, at the 75th day the polymer shell exhibited a comparatively more irregular and rougher surface, suggesting the appearance of a heterogeneous polymer texture. The observed changes might be linked to the release of a non-crosslinked polymer fraction and/or to a rearrangement of the polymer chains due to the degradation of the crosslinked shells which are exposed to water. The phase analysis (Fig. 4, panel A) highlights that the variations on the shell surface of the 75th day depend on the presence of domains which contain a different arrangement of the polymer (e.g. changes in density or crystallinity at the PVA shell surface) [53]. Probably, this finding is the consequence of a change in the weight fraction of a heterogeneous, two-component structure of the MB surface. As for a

macroscopic gel, also in the case of MBs formation the mass of PVA shell is formed by an interpenetrating polymer network where crosslinked polymer chains (the "gel" fraction) and entangled PVA segments (the "sol" fraction) coexist (i.e., by physical entanglements of the fibrils in the network). The "sol" fraction, composed by single or sparingly crosslinked chains entangled in the polymer network, is able to separate from it by elution. We attribute the slow time release of such adsorbed polymer chains as the reason being the change in the weight fraction of the PVA shells. In Section 4.2, we have discussed the possibility that the MB shell releases polymeric debris, that this release is particularly active in the first 15 days after the synthesis, and that this mass loss implies a change in the shell shear modulus $G_s$. A representative phase image obtained from a sample that was measured before the debris was removed is shown in Fig. S8, panel A, and demonstrates that such a polymer residue adsorbs onto the MB shell surface. Moreover, the presence of MBs showing a damaged shell, which can be associated with an acoustically less active "population" as mentioned in Section 4.2, was actually observed (Fig. S8, panel B).

The mass depletion of the MB shell is expected to influence both its wall thickness and its response to mechanical stimuli. The response of the MB shell to nano-mechanical solicitation was performed by point-and-shoot tapping mode AFM in a fluid environment (see Section 2.6). The corresponding force curves are shown in Fig. 4, panel B. From the analysis of the force curves, we obtained Young modulus values of $0.5 \pm 0.1$ MPa and $0.9 \pm 0.2$ MPa for the 15th day and the 75th day, respectively. The corresponding PVA shear moduli, calculated using Eq. (4), are $0.17 \pm 0.03$ MPa (day 15) and $0.30 \pm 0.07$ MPa (day 75). These values are in agreement with
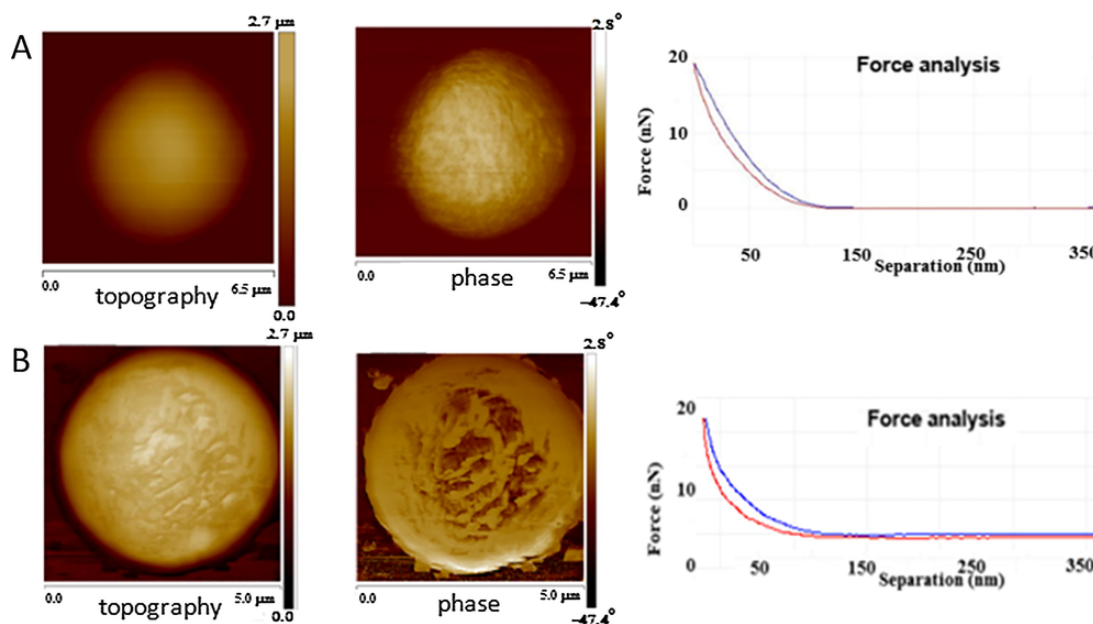
**Fig. 4.** Representative AFM images on the left and corresponding force curves on the right of PVA MBs physisorbed onto silicon substrates, acquired in water environment in the 15th (A) and the 75th days (B) after their synthesis, respectively.

**Table 2**
Morphological and mechanical parameters obtained by the AFM analysis of PVA MBs in the 15th and 75th days of ageing from three independent experiments, and at least 6 frames per measurement.

| MB parameter | day 15 | day 75 |
|---|---|---|
| Size [µm] | 3.0±0.1 | 3.0±0.1 |
| Roughness [nm] | 10.0±0.4 | 16.0±0.7 |
| Shell thickness [nm][a] | 230±1 | 200±1 |
| Young Modulus [MPa] | 0.5±0.1 | 0.9±0.2 |

[a] Measured in air.

those obtained by the acoustic analysis and reported in the literature [28,45,46]. Remarkably, this result corroborates the hypothesis that the stiffness of the MB shells significantly increases over time, consistent with the increase of the US resonance frequency reported in Table 1. It is worth noting that the agreement between $G_s$ values obtained by means of AFM and acoustic analyses is not surprising if we consider that both the applied nano-mechanical and acoustic solicitations are driven by very low amplitudes (falling within the linear elastic limit) and also by quite a similar stimulus having out-of-resonance frequency on the PVA shell. Indeed, the AFM indentation of the MB shell surface was carried out in water by setting the cantilever oscillations at ~0.2 MHz (well below the resonance frequency of the MBs). This leads the shell stress conditions to be triggered by AFM, similar to those which are used to extract the bulk modulus (at 0.5 MHz US frequency, as reported in Section 4.2).

An AFM evaluation of the MB thickness was possible only in an air environment. Under these conditions, the MBs were fractured by applying overpressure by the cantilever tip onto the MB surface. Representative bubbles' images and the associated profilometry are shown in Fig. S9. The analysis points out a thickness of the dehydrated shell of ~230 nm on day 15, which underwent a significant decrease of ~30 nm on day 75. These values are only indicative and qualitatively evaluated in accordance with an actual mass reduction of the shell thickness that was assumed for the MBs dispersed in water.

A sketch illustrating the overall hypothesised mechanism driving the ageing process of PVA MBs is reported in Fig. 5. Undoubtedly,

the shell hydration, that causes the swelling of the PVA structure [12,27,43], also contributes to the actual MBs' shell thickness as well as to the rheology and acoustics of aged PVA MBs. It has been reported that the water structured among crosslinked PVA chains can exert a significant influence on the stiffness and the stability of the polymer matrix [54–56]. The way in which the long-term modifications in the structural and mechanical properties of the PVA MBs disclosed here reflect a different dynamic of the water confined on the shell surface is an aspect that remains unclarified. Whether these considerations deserve some biomedical attention can be matter of debate, insofar as the MB surface is considered as a scaffold for controlled drug delivery.

We are confident that the morphological, viscoelastic, and acoustic characteristics and the modelling reported herein may provide a useful comparison for the surface and the interface investigation of other MB systems, especially those containing entangled polymers. It should be stressed here that our results indicate that PVA MBs exhibit a stiffness comparable to lipid MBs (16.7 N/m and 14.1 N/m, respectively), with the latter undergoing a slow stiffening in time (two months). In this respect, we hope that the results of this work will contribute further to the concept of elastomeric MBs as a subclass of polymer MBs, in which the polymer shell, appropriately crosslinked, turns into an elastic network. Thanks to this feature, elastomeric MBs, while maintaining the advantages of the "rigid" (low echogenic) polymer MBs [1] in the drug delivery field and in terms of structural stability can enhance performances in term of echogenicity and acoustic response stability.

## 5. Conclusions

Based on recent literature, polymeric MBs are gaining growing biomedical interest in terms of their high potential as US-active theranostic agents [1,2,4,7]. In this framework, a deep understanding of the mechanisms involved in the MB shells' ageing was needed.

Focusing on air-filled elastomeric PVA-shelled MBs, we demonstrated here that such agents when dispersed in water medium are found to become strongly stable over time in terms of morphology and structure, as compared to lipid-shelled MBs (months vs. hours).
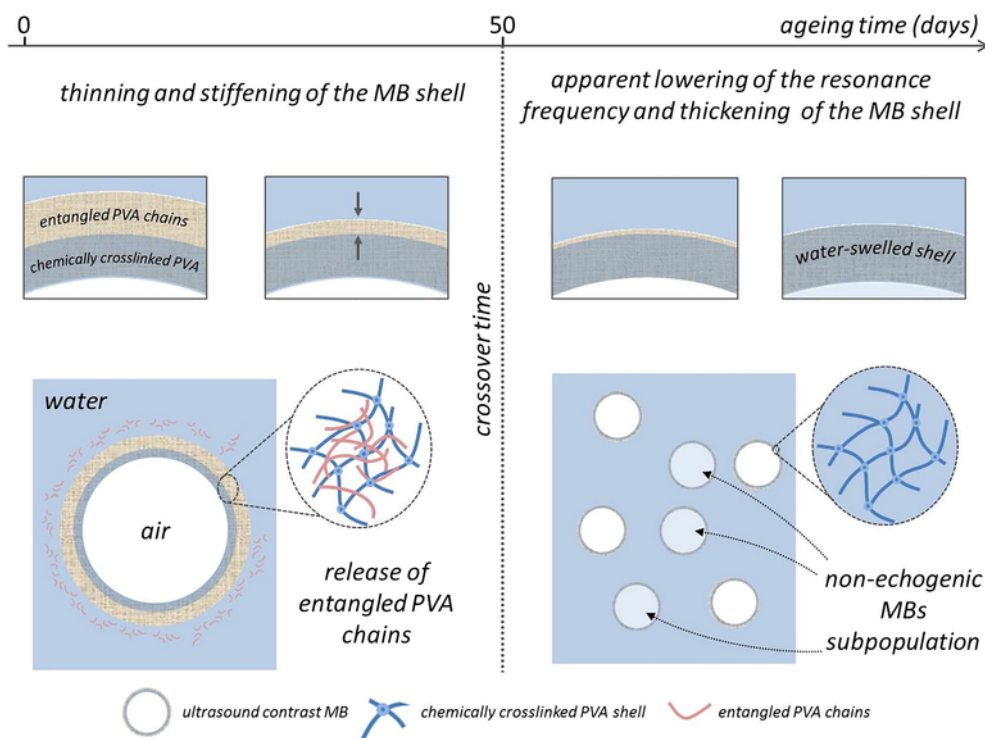
**Fig. 5.** The two mechanisms of ageing of PVA MBs are sketched in a dynamical overview with respect to the crossover time of the 50th day, as revealed by the acoustic analysis (Section 4.2). The acoustics and morphology of crosslinked PVA MBs are influenced by both the release of entangled polymer chains and the penetration of water molecules present within: the ageing of MBs is dominated by the first and the second mechanism before and after day 50th, respectively.

The system showed a good echogenicity in a range of frequencies centred at around 10 MHz, complementary to that of MBs with a lipid shell and useful to minimise the biological risks related to high-resolution imaging [11,20,57,58]. This should facilitate their use as UCAs as well as in derivatisation protocols for drug delivery and theranostics [1,7,18].

However, our results go beyond this aspect; we show here for the first time that despite the full chemical stability of the shell backbone of crosslinked PVA chains [23–26], MBs' ageing involves structural variations at the submicrometric level that affect the shell properties (i.e., thickness and viscoelasticity), the acoustic response of MBs, and their surface features at the water interface, where ligands and drugs can be bound.

Specifically, CLSM images show that PVA MBs appear intact as hollow spheres over time, retaining their size distribution. This means that cyclic hemiacetals stably link the PVA chains confined at the MB air-water interface. The combined acoustic spectroscopy in the small-oscillations regime and AFM nanomechanical characterisation provides further and deeper details. We jointly analysed, using linearised models, the phase velocity and the attenuation profiles of the US propagation in the bubbly liquid to disclose the MBs' ageing mechanisms in terms of shell thickness, viscoelastic properties, and surface morphology. We pointed out a crossover time of ∼50 days between two MBs' ageing regimes. The first one is driven by a low, progressive decrease of the MB shells' thickness due to continuous leakage of the non-crosslinked polymeric residue (removed each time by washing). Such release entails an increase in the number of crosslinks per unit of polymer mass, and, in turn, of the effective shear modulus of the shell. After the 50th day, an apparent turnaround is observed most likely due to the presence of a MB subpopulation of non-echogenic systems which alter the attenuation cross section of the overall system.

In brief, the overall results indicate that the PVA shell can be identified as being formed by an interpenetrating polymer network of crosslinked polymer chains and entangled PVA segments, the latter being slowly released after washing in the water environment. This is the cause behind the MBs' ageing up to the 50th day. Thereafter, the presence of a minor population of acoustically inactive MBs should be taken into account.

The modifications in the MBs' acoustic response to megasonic fields reported here are not dramatic, but can also affect MBs whose shells are made up of different polymers, particularly if they are entangled [1]. We are confident that our case study will be helpful to characterise the ageing processes of such systems for several weeks after the preparation, allowing to optimise their echogenic and therapeutic properties. In a forthcoming work, we will investigate the time-related stability of PVA MBs in the non-linear oscillations regime, which is employed in both second harmonic imaging and drug delivery [5,59]. The effects of shell functionalisation (with ligands and/or drugs) on the MBs' stability will be also accounted for, at the interface containing cells or even with other solid surfaces as echogenic devices for *in situ* release. In this respect, this present study is of pivotal importance, since the specific morphological and initial mechanical conditions of PVA shells are undoubtedly involved in the MBs' stability with respect to either US irradiation or surface derivatisation.

## Appendix A. Supplementary material

Supplementary data to this article can be found online at https://doi.org/10.1016/j.jcis.2018.12.110.

## References

[1] S.R. Sirsi, M.A. Borden, State-of-the-art materials for ultrasound-triggered drug delivery, Adv. Drug Deliv. Rev. 72 (2014) 3–14.

[2] H. Lee, H. Kim, H. Han, M. Lee, S. Lee, H. Yoo, J.H. Chang, H. Kim, Microbubbles used for contrast enhanced ultrasound and theragnosis: a review of principles to applications, Biomed. Eng. Lett. 7 (2017) 59–69.

[3] D. Cosgrove, Ultrasound contrast agents: an overview, Eu. J. Rad. 60 (2006) 324–330.

[4] K.-H. Song, B.K. Harvey, M.A. Borden, State-of-the-art of microbubble-assisted blood-brain barrier disruption, Theranostics 8 (16) (2018) 4393–4408.

[5] M.C. Cochran, J. Eisenbreya, R.O. Ouma, M. Soulen, M.A. Wheatley, Doxorubicin and paclitaxel loaded microbubbles for ultrasound triggered drug delivery, Int. J. Pharm. 414 (2011) 161–170.

[6] L. Fu, H.-T. Ke, Nanomaterials incorporated ultrasound contrast agents for cancer theranostics, Cancer. Biol. Med. 13 (2016) 313–324.

[7] L. Oddo, B. Cerroni, F. Domenici, A. Bedini, F. Bordi, E. Chiessi, S. Gerbes, G. Paradossi, Next generation ultrasound platforms for theranostics, J. Colloid Interface Sci. 491 (2017) 151–160.

[8] M.W. Keller, W. Glasheen, S. Kaul, Albunex: a safe and effective commercially produced agent for myocardial contrast echocardiography, J. Am. Soc. Echocardiogr. (1989) 248–252.

[9] L.J. Jablonowski, M.C. Cochran, J.R. Eisenbrey, N.T. Teraphongphom, M.A. Wheatley, Shell effects on acoustic performance of a drug-delivery system activated by ultrasound, J. Biomed. Mater. Res. Part A: Off. J. Soc. Biomater., Japanese Soc. Biomater. Aust. Soc. Biomater. Korean Soc. Biomater. 105A (2017) 3189–3196.

[10] D.M. El-Sherif, J.D. Lathia, N.T. Le, M.A. Wheatley, Ultrasound degradation of novel polymer contrast agents, J. Biomed. Mater. Res. Part A 68 (1) (2004) 71–78.

[11] B. Cerroni, R. Cicconi, L. Oddo, M. Scimeca, R. Bonfiglio, R. Bernardini, G. Palmieri, F. Domenici, E. Bonanno, M. Mattei, G. Paradossi, In vivo biological fate of poly(vinyl alcohol) microbubbles in mice. Heliyon 4 (2018) 1.

[12] G. Tzvetkov, B. Graf, Paulo Fernandes, A. Fery, F. Cavalieri, G. Paradossi, In situ imaging of gas-filled microballoons by soft X-ray spectromicroscopy, Soft Matter 4 (2008) 510.

[13] E. Talu, K. Hettiarachchi, S. Zhao, R.L. Powell, A.P. Lee, M.L. Longo, P.A. Dayton, Tailoring the size distribution of ultrasound contrast agents: possible method for improving sensitivity in molecular imaging, Mol. Imaging. 6 (2007) 384–392.

[14] C.C. Chen, S.-Y. Wu, J.D. Finan, B. Morrison 3rd, E.E. Konofagou, An experimental study on the stiffness of size-isolated microbubbles using atomic force microscopy, IEEE Trans. Ultrason. Ferroelectr. Freq. Control. 60 (2013) 524–534.

[15] V. Sboros, S.E. Glynos, S.D. Pye, C.M. Moran, M. Butler, J. Ross, R. Short, W.N. McDicken, V. Koutsos, Nanointerrogation of ultrasonic contrast agent microbubbles using atomic force microscopy, Ultrasound Med. Biol. 32 (2006) 579–585.

[16] G. Bonacucina, D.R. Perinelli, M. Cespi, L. Casettari, R. Cossi, P. Blasia, G.F. Palmieri, Acoustic spectroscopy: a powerful analytical method for the pharmaceutical field?, Int. J. Pharm. 503 (2016) 174–195.

[17] H. Mulvana, R.J. Browning, Y. Luan, N. de Jong, M.-X. Tang, R.J. Eckersley, E. Stride, Characterization of contrast agent microbubbles for ultrasound imaging and therapy research, IEEE Trans. Ultrason. Ferroelectr. Freq. Control. (2017) 232–251.

[18] F. Cavalieri, E. Chiessi, R. Villa, L. Viganò, N. Zaffaroni, M.F. Telling, G. Paradossi, Novel PVA-based hydrogel microparticles for doxorubicin delivery, Biomacromolecules 9 (2008) 1967–1973.

[19] D. Grishenkov, L. Kari, L.-Å. Brodin, T.B. Brismar, G. Paradossi, In vitro contrast-enhanced ultrasound measurements of capillary microcirculation: Comparison between polymer- and phospholipid-shelled microbubbles, Ultrasonics 51 (2011) 40–48.

[20] S. Mitragotri, Healing sound: the use of ultrasound in drug delivery and other therapeutic applications, Nat. Rev. Drug. Discov. 4 (255) (2005) 260.

[21] Y. Toumia, F. Domenici, S. Orlanducci, F. Mura, D. Grishenkov, P. Trochet, S. Lacerenza, F. Bordi, G. Paradossi, Graphene meets microbubbles: a superior contrast agent for photoacoustic imaging, Appl. Mater. Interfaces 8 (2016) 16465–16475.

[22] F. Cavalieri, A. El Hamassi, E. Chiessi, G. Paradossi, Stable polymeric microballoons as multifunctional device for biomedical uses: synthesis and characterization, Langmuir 21 (2005) 8758–8764.

[23] D.B.G. Williams, A. Cullen, A. Fourie, H. Henning, M. Lawton, W. Mommsen, P. Nangu, J. Parker, A. Renison, Mild water-promoted selective deacetalisatison of acyclic acetals, Green Chem. 12 (2010) 1919–1921.

[24] N. Nakamura, K. Suzuki, Study on ketalization reaction of poly(vinyl alcohol) by ketones. VIII. kinetic study on acetalization and ketalization reactions of poly(vinyl alcohol), J. Polym. Sci. A Polym. Chem. 34 (1996) 3319–3327.

[25] A. Piasecki, Hydrolysis of 2-[2-(ω-Hydroxyalkoxy)alkyl]-substituted 1,3-dioxolanes and 1,3-dioxanes in aqueous solution of hydrochloric acid, J. f. prakt. Chemie 327 (1985) 731–738.

[26] A. Sokolowski, B. Burczyk, Hydrolysis- isomerization of 2-alkyl-5-hydroxy-1,3-dioxanes and 2-alkyl-4-hydroxymethyl-l,3-dioxolanes in aqueous solution of hydrochloric acid, J. f. prakt. Chemie. 323 (1981) 63–72.

[27] F. Saglimbeni, S. Bianchi, G. Bolognesi, G. Paradossi, R. Di Leonardo, Optical characterization of an individual polymer-shelled microbubble structure via digital holography, Soft Matter 8 (2012) 8822–8825.

[28] D. Grishenkov, C. Pecorari, T.B. Brismar, G. Paradossi, Characterization of acoustic properties of PVA-shelled ultrasound contrast agents: ultrasound-induced fracture (part II), Ultrasound Med. Biol. 35 (2009) 1139–1147.

[29] S.V. Kothapalli, V. Daeichin, F. Mastik, L.A. Brodin, B. Janerot-Sjoberg, G. Paradossi, N. de Jong, D. Grishenkov, Unique pumping-out fracturing mechanism of a polymer-shelled contrast agent: an acoustic characterization and optical visualization, IEEE Trans. Ultrason. Ferroelectr. Freq. Control 62 (3) (2015) 451–462.

[30] L. Hoff, Acoustic Characterization of Contrast Agents for Medical Ultrasound Imaging, Springer, 2001.

[31] H.W. Hao, A.M. Barò, J.J. Saenz, Electrostatic and contact forces in force microscopy, J. Vac. Sci. Technol. B 9 (1991) 1323.

[32] B. Cappella, G. Dietler, Force-distance curves by atomic force microscopy, Surf. Sci. Rep. 34 (1999) 1–3.

[33] J.P. Aimé, Z. Elkaakour, C. Odin, T. Bouhacina, D. Michel, J. Curely, A. Dautant, Comments on the use of the force mode in atomic force microscopy for polymer films, J. Appl. Phys. 76 (1994) 754.

[34] G.N. Greaves, A.L. Greer, R.S. Lakes, T. Rouxel, Poisson's ratio and modern materials, Nat. Mater. 10 (2011) 823–837.

[35] B.V. Derjaguin, V.M. Müller, Y.P. Toporov, Effect of contact deformations on the adhesion of particles, J. Colloid Interface Sci. 53 (1975) 314–326.

[36] L.D. Landau, E.M. Lifshitz, Fluid Mechanics, second ed., Butterworth-Heineman, Oxford, U.K, 1987.

[37] L. Hoff, P.C. Sontum, J.M. Hovem, Oscillations of polymeric microbubbles: effect of the encapsulating shell, J. Acoust. Soc. Am. 107 (2000) 2272–2280.

[38] A.A. Doinikov, A. Bouakaz, Review of shell models for contrast agent microbubbles, IEEE Trans. Ultrason. Ferroelectr. Freq. Control. 58 (2011) 981–993.

[39] G. Tzvetkov, P. Fernandes, S. Wenzel, A. Fery, G. Paradossi, R.H. Fink, Soft X-ray induced modifications of PVA-based microbubbles in aqueous environment: a microspectroscopy study, Phys. Chem. Chem. Phys. 11 (2009) 1098–1104.

[40] M. Poehlmann, D. Grishenkov, S.V.V.N. Kothapalli, J. Härmark, H. Hebert, A. Philipp, R. Hoeller, M. Seuss, C. Kuttner, S. Margheritelli, G. Paradossi, A. Fery, On the interplay of shell structure with low- and high-frequency mechanics of multifunctional magnetic microbubbles, Soft Matter 10 (2014) 214–226.

[41] J. Härmark, H. Hebert, P.J.B. Koeck, Shell thickness determination of polymer-shelled microbubbles using transmission electron microscopy, Micron 85 (2016) 39–43.

[42] T.G. Leighton, The Acoustic Bubble, first ed., Academic Press Ltd., London, UK, 1994.

[43] P.A.L. Fernandes, G. Tzvetkov, R.H. Fink, G. Paradossi, A. Fery, Quantitative analysis of scanning transmission x-ray microscopy images of gas-filled PVA-based microballoons, Langmuir 24 (2008) 13677–13682.

[44] J.W. Strutt Baron, The Theory of Sound, Vol. 2., Dover Publications, New York, USA, 1945.

[45] D. Grishenkov, C. Pecorari, T.B. Brismar, G. Paradossi, Characterization of acoustic properties of PVA-shelled ultrasound contrast agents: linear properties (part I), Ultrasound Med. Biol. 35 (2009) 1127–1138.

[46] S. Capece, F. Domenici, F. Brasili, L. Oddo, B. Cerroni, A. Bedini, F. Bordi, E. Chiessi, G. Paradossi, Complex interfaces in ''phase-change'' contrast agents, Phys. Chem. Chem. Phys. 18 (2016) 8378–8388.

[47] R. Thurasingham, Sound speed in bubbly water at megahertz frequencies, Ultrasonics 36 (1998) 767–773.

[48] H. Hertz, Über die Berührung fester elastischer Körper, J. Reine. Angew. Math. 92 (1881) 156.

[49] W.C. Oliver, G.M. Pharr, Measurement of hardness and elastic modulus by instrumented indentation: Advances in understanding and refinements to methodology, J. Mat. Res. 19 (2004) 3–20.

[50] Y. Garini, B.J. Vermolen, I.T. Young, From micro to nano: recent advances in high-resolution microscopy, Curr. Opin. Biotechnol. 16 (2005) 3–12.

[51] A. Charlesby, Elastic modulus formulae for a crosslinked network, Radiat. Phys. Chem. 40 (1992) 117–120.

[52] P.J. Flory, Principles of Polymer Chemistry, Cornell University Press, New York, USA, 1953.

[53] Z. Ye, X. Zhao, Phase imaging atomic force microscopy in the characterization of biomaterials, J. Microsc. 238 (2010) 27–35.

[54] G. Tesei, G. Paradossi, E. Chiessi, Influence of surface concentration on poly(vinyl alcohol) behavior at the water–vacuum interface: a molecular dynamics simulation study, J. Phys. Chem. B 118 (2014) 6946–6955.

[55] G. Paradossi, F. Cavalieri, E. Chiessi, M.T.F. Telling, Super-cooled water in PVA matrices: I. An incoherent Quasi Elastic Neutron Scattering (QENS) study, J. Phys. Chem. B 107 (2003) 8363–8371.

[56] E. Chiessi, G. Paradossi, F. Cavalieri, Super-cooled water in PVA matrices: II. A molecular dynamics simulation study and comparison with QENS results, J. Phys. Chem. B 109 (2005) 8091–8096.

[57] F. Domenici, F. Brasili, S. Giantulli, B. Cerroni, A. Bedini, C. Giliberti, R. Palomba, I. Silvestri, S. Morrone, G. Paradossi, M. Mattei, F. Bordi, Differential effects on membrane permeability and viability of human keratinocyte cells undergoing very low intensity megasonic fields, Sci. Rep. 7 (16536) (2017) 1–10.

[58] F. Domenici, C. Giliberti, A. Bedini, R. Palomba, I. Udroiu, L. Di Giambattista, D. Pozzi, S. Morrone, F. Bordi, A. Congiu Castellano, Structural and permeability sensitivity of cells to low intensity ultrasound: Infrared and fluorescence evidence in vitro, Ultrasonics 54 (2014) 1020–1028.

[59] G. Lajoinie, Y. Luan, E. Gelderblom, B. Dollet, F. Mastik, H. Dewitte, I. Lentacker, N. de Jong, M. Versluis, Non-spherical oscillations drive the ultrasound-mediated release from targeted microbubbles, Commun. Phys. 1 (22) (2018) 1–9.